Optimized KinectFusion Algorithm for 3D Scanning Applications

Faraj Alhwarin, Stefan Schiffer, Alexander Ferrein and Ingrid Scholl
Mobile Autonomous Systems & Cognitive Robotics Institute (MASCOR),
FH Aachen University of Applied Sciences, Aachen, Germany

Keywords: Optimized KinectFusion, Body Scanner, 3D Reconstruction.

Abstract: KinectFusion is an effective way to reconstruct indoor scenes. It takes a depth image stream and uses the iterative closests point (ICP) method to estimate the camera motion. Then it merges the images in a volume to construct a 3D model. The model accuracy is not satisfactory for certain applications such as scanning a human body to provide information about bone structure health. For one reason, camera noise and noise in the ICP method limit the accuracy. For another, the error in estimating the global camera poses accumulates. In this paper, we present a method to optimize KinectFusion for 3D scanning in the above scenarios. We aim to reduce the noise influence on camera pose tracking. The idea is as follows: in our application scenarios we can always assume that either the camera rotates around the object to be scanned or that the object rotates in front of the camera. In both cases, the relative camera/object pose is located on a 3D-circle. Therefore, camera motion can be described as a rotation around a fixed axis passing through a fixed point. Since the axis and the center of rotation are always fixed, the error averaging principle can be utilized to reduce the noise impact and hence to enhance the 3D model accuracy of scanned object.

1 INTRODUCTION

3D reconstruction is one of the most fundamental issues in computer vision, which has many practical applications in a range of fields such as robotics, virtual reality, video games and 3D scanning. To reconstruct a scene, a sequence of images captured at different viewpoints or a video is usually required. Generally, for visual 3D reconstruction, two problems have to be solved: (1) camera motion tracking and (2) depth recovery from 2D images. For camera tracking, the camera has to move slightly over time or its frame-rate has to be sufficient, so that successive images overlap. The relative camera motion from frame to frame can then be computed by feature extraction and matching. This technique is known as Structure from Motion (SfM) (Changchang, 2013; Moulon et al., 2013). For scene depth recovery from 2D images, the scene has to be viewed from at least two known viewpoints. Stereo correspondences can then be used for depth estimation using epipolar geometry and stereo triangulation. This technique is called Multi view Stereo (MVS) (Furukawa and Ponce, 2007; Hernández et al., 2007).

By combining SfM and MVS, visual 3D reconstruction can be realized. Once the camera motion is estimated, recovered depth frames are transformed according to their corresponding camera poses and combined together or merged into a common 3D volume to generate a 3D model of the scene. For camera motion refinement, bundle adjustment or pose graph optimization are usually used (Ni et al., 2007; Yu and Zhang, 2016).

According to feature density used for camera tracking and depth recovering, 3D reconstruction methods can be classified into two major categories: *sparse* and *dense* reconstruction. By sparse reconstruction, the camera motion as well as scene depth are estimated by matching sparse local features extracted from the images. The accuracy of camera tracking is strongly dependent on the texture content of the scene. In addition, the generated model is incomplete and its quality is poor because only depths of sparsely distributed features are used. Although sparse methods such as monocular SLAM (Schoeps et al., 2014; Davison et al., 2007) are successfully used in robotics, e.g. for self-localisation and mapping, they are totally unsuitable for 3D scanning applications. With dense approaches, sparse features are first used to estimate initial camera motion. Then the depth of all image points computed by stereo vision (Negre et al., 2016; Engel et al., 2015) or provided by

Alhwarin, F., Schiffer, S., Ferrein, A. and Scholl, I.
Optimized KinectFusion Algorithm for 3D Scanning Applications.
DOI: 10.5220/0006594700500057
In *Proceedings of the 11th International Joint Conference on Biomedical Engineering Systems and Technologies (BIOSTEC 2018) - Volume 2: BIOIMAGING*, pages 50-57
ISBN: 978-989-758-278-3

a depth sensor like the Microsoft Kinect (Kerl et al., 2013; Fioraio and Stefano, 2014) are used to refine camera poses. While the scene can be reconstructed completely with dense approaches, the accuracy of reconstructed model is insufficient for 3D body scanning and the run time is extremely expensive.

Using KinectFusion method (Newcombe et al., 2011), it is possible to determine camera motion from depth images of a Kinect sensor of Microsoft in real time and simultaneously to create a 3D model of the scene by integrating depth information into a truncated signed distance function (TSDF) volume. Using the Iterative Closest Point (ICP) method, correspondences in 3D point clouds are found and used for camera motion tracking. In contrast to other 3D reconstruction methods that track camera movement from frame to frame, KinectFusion tracks camera motion from frame to model increasing the reliability of tracking, since depth noise is reduced while reconstructing model by averaging of all previous depth frames. In KinectFusion, finding correspondences, estimating camera motion and generating 3D model can be parallelized efficiently on GPU hardware, which makes it real-time adaptable.

Generally, KinectFusion has two main drawbacks. The first one is that the reconstruction fails if the scene has no distinctive shapes, for example, when the camera moves parallel to a plane or rotates around cylindrical or spherical surface. In such cases, KinectFusion can not track the camera motion correctly. This problem can be faced by human body scanning applications for medical purpose, where many parts of naked human body are approximately cylindrical such as legs and the torso. The second drawback is that the depth data provided by the Kinect sensor involve error in a range of $\pm 5mm$. In camera motion tracking this error causes small local drifts that are accumulated over time. This in turn leads to unacceptable deformations in the resulting 3D model.

Recently, many improvements of KinectFusion method have been proposed. (Jia et al., 2016) improved KinectFusion by adding graph based-optimization to achieve rapid optimization of error accumulation. (Afzal et al., 2014) proposed a modification of KinectFusion to enhance 3D reconstruction of non-rigidly deforming objects. (Kainz et al., 2012) improved the KinectFusion algorithm to allow for 3D reconstruction from multiple sensors simultaneously. (Whelan et al., 2012) extended the KinectFusion method by visual odometry to avoid camera motion tracking failure at regions of low geometric features. (Pagliari et al., 2014) proposed an improvement of KinectFusion by executing the scanning process twice. In the first run, an average circular trajectory of the camera is estimated. In the second run, the trajectory is used for depth data correction.

In this paper, we present a new method to optimize KinectFusion for a 3D body scanner. The idea is based on the assumption that, for most 3D scanning applications, the camera rotates about the object to be scanned or the object rotates in front of the camera. In both cases, the rotation axis and the rotation center remain unchanged while scanning. Therefore, the camera motion tracking can be simplified by estimating a rotation angle instead of estimating a 6 DoF transformation. The rotation axis and center are determined accurately by averaging of depth errors. Performing camera motion tracking using our method improves the quality of reconstructed 3D model for two reasons. For one, only angle errors are accumulated, instead of accumulating transformation drifts. For another, reducing correspondence search to only one dimension removes many outliers. The rest of paper is organized as follows. In Section 2 the KinectFusion method is described briefly. In Section 3, our method is presented in detail. Experimental results are evaluated in Section 4. Finally, the paper concludes in Section 5.

2 KINECT FUSION ALGORITHM

KinectFusion (Newcombe et al., 2011; Izadi et al., 2011) is a powerful 3D reconstruction technique based on Microsoft Kinect Sensor. It allows the 3D reconstruction of an indoor scene through moving a kinect camera around in real-time using commodity graphics hardware. It integrates and merges consecutive depth images provided by the Kinect depth sensor in a 3D volumetric data structure, assuming the relative position between the sensor and the object is only slightly changed over time. As described in (Newcombe et al., 2011), KinectFusion consists of four major stages: surface measurements, surface reconstruction update, surface prediction and sensor pose estimation. In the surface measurement stage the vertex and normal maps are computed from the depth image and the camera's intrinsic parameters. Before computing vertex and normal maps, depth images are filtered using bilateral filter to reduce depth noise while keeping depth edges unblurred as much as possible. In the surface reconstruction update, the surface measurements computed in the previous stage are transformed according to a global coordinate frame and integrated into a 3D volumetric data structure called Truncated Signed Distance Function (TSDF). For sensor pose estimation, it is assumed that only a small camera motion occurs from one frame to the next. This allows the use of a fast projective data association algorithm (Arya et al., 1995) to obtain correspondence points and the point-plane metric (Yang and Gerard, 1992) for sensor pose estimation.

3 OPTIMIZED KINECT FUSION

As mentioned above, in our target applications for 3D scanning, the camera usually rotates around the object to be scanned or the object rotates in front of the camera. In both cases the relative object/camera motion trajectory is described as a three-dimensional circle. Therefore, the camera pose is always described as a rotation by a variable angle (rotation angle) about a fixed axis (rotation axis) passing through a fixed point (rotation center). In KinectFusion, the Iterative Closest Points (ICP) method is used to estimate the transformation between each successive depth images (the current depth image and a ray-casted depth image from the live reconstructed 3D model from all previous depth images). The transformation consists of six parameters, three for the rotation and three for the translation. Since the depth data is noisy, this will affect all transformation parameters. In our proposed method, in order to reduce the noise effect on the estimated transformation as much as possible, the transformation is separated into three components: (1) the axis, (2) the center and (3) the angle of rotation. Since the axis and the center of rotation are fixed for all camera poses, they can be estimated offline and error averaging can be applied to reduce depth noise effects on them significantly. Through this idea, the effect of noise is only limited to the rotation angle, rather than affecting all the transformation parameters, which allows to reduce the error of camera motion estimation and to increase the quality of the generated 3D model. For this purpose we must firstly determine the axis and the center of rotation with a reasonable accuracy. Then we use the ICP method to estimate only the rotation angle between successive camera frames. The determination of rotation axis and center is only needed once, as long as the set-up of the scanner is not changed.

3.1 Determination of Rotation Axis and Center

To determine the axis and center of rotation while reducing the noise effect on them, a sphere with a known radius and a specific color is used. We rotate the sphere in front of the kinect camera and estimate the sphere centers in the successive camera frames. From each depth image and its corresponding color image, a colored point cloud is computed. Color-based segmentation is used to segment the point cloud keeping only points lying on the sphere. A spherical surface with a certain radius is then fitted to the remaining points. Figure 1 shows the input point cloud, the color-based segmented point cloud, and the fitted spherical surface.

In the ideal case, these sphere centers should all fall on a 3D circle, but because of depth noise, a circular point cloud is obtained as shown in Figure 2(a). Using the Random Sample Consensus (RANSAC) method, several circles can be fitted to this point cloud. The error can be averaged over all these circles by computing the mean circle. The mean circle axis and center represent the rotation axis and center of the scanner. Figure 2(b) shows a range of circles fitted to center cloud and the computed mean circle.

Table 1 shows the mean values of the rotation axis and center and their standard deviations. Once the rotation axis and center of the scanner are known, camera motion estimation can be reduced to estimate only one parameter (i.e. the rotation angle) rather than estimating 6 DoF transformation, as the case of KinectFusion. For this purpose, in the next section, we will modify camera tracking stage of KinectFusion taking into account that the axis and center of rotation are previously known.

3.2 Rotation Angle Estimation

Assuming that the camera pose at any time is given by a rotation about a known axis passing through a known point. Hence, the rotation matrix and translation vector are given as:

$$R = \begin{bmatrix} r_1^2.q+c & r_1r_2.q-r_3.s & r_1r_3.q+r_2.s \\ r_1r_2.q+r_3.s & r_2^2.q+c & r_2r_3.q-r_1.s \\ r_1r_3.q-r_2.s & r_2r_3.q+r_1.s & r_3^2.q+c \end{bmatrix} \quad (1)$$

$$t = o - R\cdot o$$

where $c = cos\alpha$, $s = sin\alpha$, $q = (1 - cos\alpha)$, $r = [r_1, r_2, r_3]^T$ is normalized rotation axis, and $o = [o_1, o_2, o_3]^T$ is rotation center. This transformation maps any 3D point p_c^k in camera frame at time k to its corresponding point p_g^k in global coordinate frame.

$$p_g^k = R\cdot p_c^k + t = R\cdot(p_c^k - o) + o \quad (2)$$

By substituting Equation 1 in Equation 2 and rearranging we get

$$p_g^k = A_g^k \cdot cos\alpha + B_g^k \cdot sin\alpha + C_g^k \quad (3)$$

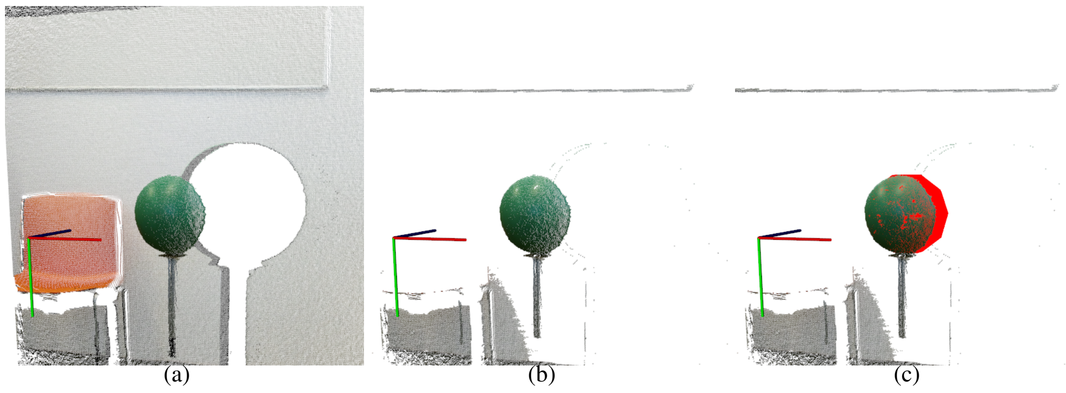
Figure 1: Computation sphere center: (a)input point cloud, (b)color-based segmented point cloud and (c) spherical surface fitted to segmented point cloud.

Table 1: mean values and standard deviations of averaged 3D circles.

Averaged circle	Circle axis			Circle center		
	x	y	z	x	y	z
mean value	0.4964	0.5852	0.6359	-0.0232	0.9986	-0.0463
std deviation	0.0046	0.0017	0.0049	0.0048	0.0002	0.0051

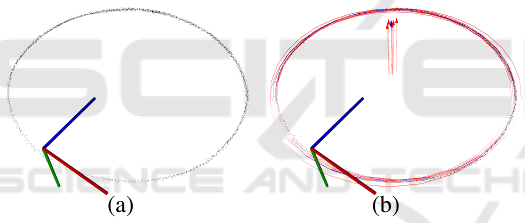
Figure 2: (a) Sphere centers obtained while moving it in front of the kinect sensor represented as pointcloud and (b) some fitted circles using RANSAC and their axes represented as arrows (red circles) and mean circle (blue).

where
$A_g^k = (I_{3x3} - rr^T)(p_c^k - o)$
$B_g^k = [r]_x(p_c^k - o)$
$C_g^k = rr^T(p_c^k - o) + o$
with

$$[r]_x = \begin{bmatrix} 0 & -r_3 & r_2 \\ r_3 & 0 & -r_1 \\ -r_2 & r_1 & 0 \end{bmatrix}$$

As in KinectFusion, for camera motion tracking we use the projective data association method to detect correspondences points and the point-plane error metric for camera pose estimation. Utilising the vertex and normal maps computed from current depth frame and the depth frame ray-casted from TSDF volume, the current camera pose can be estimated by minimizing the following point-plane energy function(Newcombe et al., 2011).

$$E(\alpha) = \sum_u \left[(p_g^k(u) - \hat{q}_g^{k-1}(\hat{u}))\hat{n}_g^{k-1}(\hat{u}) \right]^2 \quad (4)$$

where $p_g^k(u)$ are 3D points at xy-position u sensed by camera at time k and transformed to global frame, $\hat{q}_g^{k-1}(\hat{u})$ and $\hat{n}_g^{k-1}(\hat{u})$ are corresponding 3D points and its normals predicted from the 3D model at time k-1. To reduce outliers, two constraints are considered: Firstly, correct correspondences must have the same distance to the rotation center.

$$\left| \left\| (p_g^k(u) - o) \right\|_2 - \left\| \hat{q}_g^{k-1}(\hat{u}) - o \right\|_2 \right| <= Thr_1$$

and secondly, correct correspondences must lie on the same plane perpendicular to the rotation axis.

$$(p_g^k(u) - \hat{q}_g^{k-1}(\hat{u})) \cdot r <= Thr_2$$

Only correspondences that meet these two conditions are taken into consideration while computing the objective function $E(\alpha)$.

By substituting Equation 3 in Equation 4 we get

$$E(\alpha) = \sum_u [(a \cdot cos\alpha + b \cdot sin\alpha + c)]^2 \quad (5)$$

where
$n = \hat{n}_g^{k-1}(\hat{u})$
$a = (A_g^k)^T \cdot n$
$b = (B_g^k)^T \cdot n$
$c = (C_g^k - \hat{q}_g^{k-1}(\hat{u}))^T \cdot n$

By expanding Equation 5 we can get

$$E(\alpha) = cos^2\alpha \cdot \sum a^2 + sin^2\alpha \cdot \sum b^2 + \sum c^2 + 2cos\alpha sin\alpha \cdot \sum ab + 2sin\alpha \cdot \sum bc + 2cos\alpha \cdot \sum ac \quad (6)$$

By computing the derivative of the function $E(\alpha)$ with respect to α and setting to zero, we get

$$\begin{aligned} f(\alpha) &= \frac{dE(\alpha)}{d\alpha} \\ &= sin(2\alpha) \cdot (\sum b^2 - \sum a^2) + 2cos(2\alpha) \cdot \sum ab + 2cos(\alpha) \cdot \sum bc - 2sin(\alpha) \cdot \sum ac \\ &= 0 \end{aligned} \quad (7)$$

The summands in Equation 7 are computed on GPU using a parallel tree-based reduction (Harris et al., 2007). By solving Equation 7 we get the rotation angle that minimizes the point to plane metric. To solve this equation, we use the Newton-Raphson method.

$$\alpha_k = \alpha_{k-1} - f(\alpha_{k-1})/f'(\alpha_{k-1}) \quad (8)$$

Assuming angle between each two successive camera frames is small, choosing $\alpha_0 = 0$ is a good start for rapid convergence of the solution.

4 EXPERIMENTAL RESULTS

In order to evaluate the performance of our proposed method, we conducted some comparative experiments in regards to the standard KinectFusion. In these experiments we used the open source implementation of KinectFusion provided in the Point Cloud Library (PCL) called KinFu. In our implementation, we used KinFu code as a base and modified it according to our proposed idea explained in Section 3 above. To access the depth data generated by the Kinect v2 camera, the $iai-kinect2$ (Wiedemeyer, 2015) was used. The $iai-kinect2$ is a software wrapper that bridges the open source driver *libreenect2* for Kinect v2 devices with Robot Operating System (ROS) and involves tools for camera calibration and registration.

In the first experiment, we used a display dummy, that simulates a human body. The dummy was scanned with Comet L3D scanner with resolution of 0.1 mm and the created 3D model (shown in Figure 3(a))is used as a ground truth.
The scanning was realized by rotating the dummy in front of kinect camera using a turntable. To compare our method to KinectFusion, the depth frames are stored while scanning, and used offline to reconstruct 3D meshes using standard KinFu and our optimized KinFu. The obtained meshes are presented in Figures 3(b) and 3(c). We found that the quality of meshes reconstructed by our method are always better than the meshes of standard KinFu. As shown in Figure 3(d), some parts (such as hands) are deformed in KinFu meshes, while they are reconstructed correctly in optimized meshes(see Figure 3(e)).

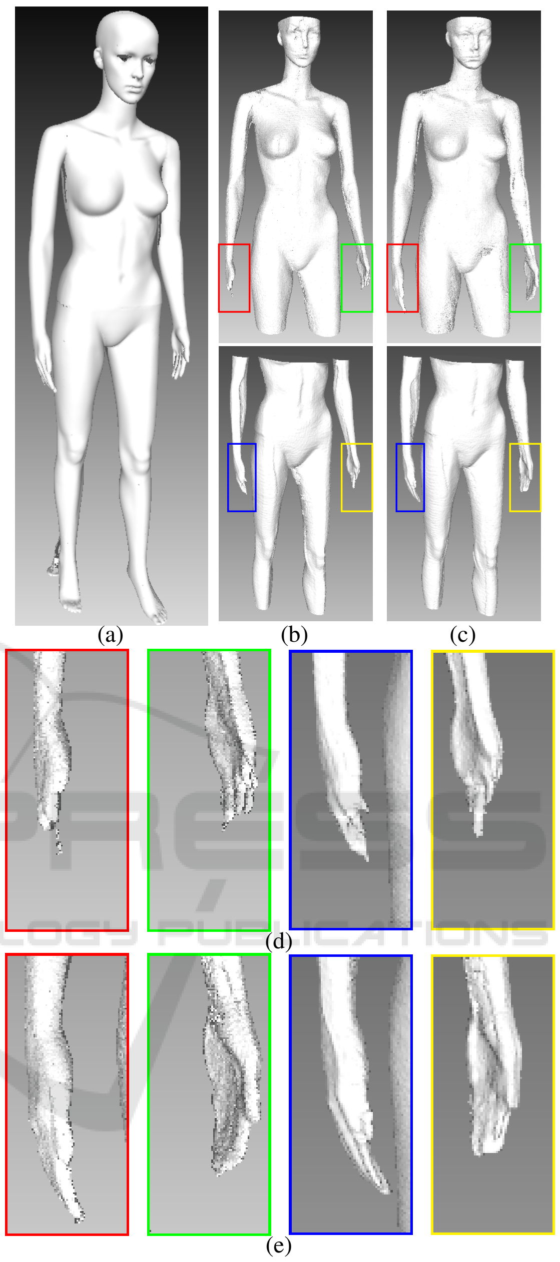

Figure 3: 3D models of the display dummy used in our experiments. (a) model of the dummy scanned by laser scanner and used as ground truth. (b) model of dummy scanned with standard KinectFusion. (c) model of dummy scanned with our optimized KinectFusion (d) zoom of some parts in standard KinectFusion meshes. (e) zoom of the same parts in optimized KinectFusion meshes.

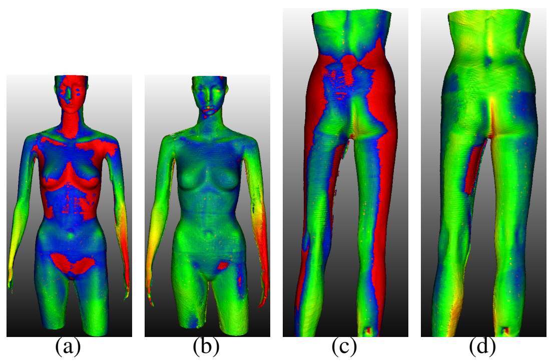

Figure 4: The point to point comparison between ground truth mesh and KinFu meshes (a)+(c) and optimized KinFu mesh (b)+(d), visualized by color scale.

To compare meshes quantitatively, the point to point distances between obtained meshes and ground truth mesh are computed using CloudCompare software (Girardeau-Montaut, 2014). The distances are visualized as color scale ranging from blue (<-5mm) via green (0mm) to red (>5mm) in Figure 4 and represented as histograms in Figure 5. As evident from the histograms, our method outperforms the standard KinectFusion. For our meshes more than 80% of point distances are lying within the range ± 5mm, whereas for the original KinFu meshes only less than 50% are lying in the same range. In the Figures 4(a, b) and first row of Figures 5, it shown that many points have distances larger than 5mm. The reason of that is because the arms of the dummy are movable and differ from the ground truth model.

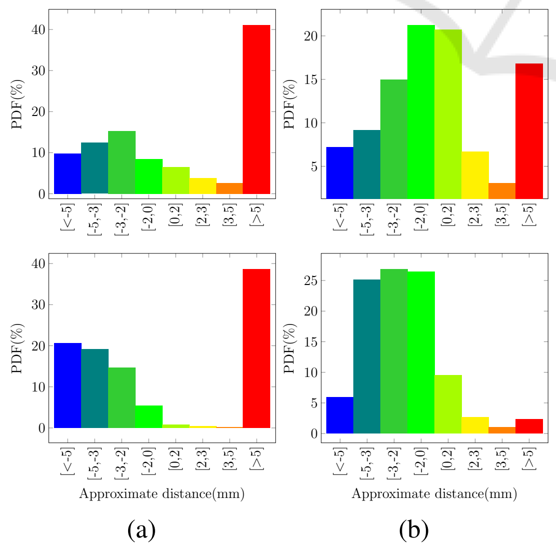

Figure 5: Distance histograms for standard KinFu meshes (a) and optimized KinFu meshes (b).

During our experiments, we found that standard KinectFusion always deforms the model of scanned object by down-scaling it non-linearly. The same result was found in (Pagliari et al., 2014), where they interpreted it as a cause of focal length error of the depth sensor. In this paper, we found that the reason of downscaling is due to the accumulation of depth data errors. Using our optimization we reduced this effect significantly as shown in Fig. 6 and Fig. 7. In Figure 6 meshes are reconstructed from the same depth frame sequence and at the same fusion parameters (voxel grid size, truncated threshold and etc) using standard and optimized KinFu. Meshes are then registered to a ground truth mesh and some slices are taken to show scaling effect. Figure 7 shows the 2D views of the slices visible as thin yellow boxes in Figure 6(d). As evident from the slices shown in Figure 7 it is clear that the optimized mesh is closer to the ground truth mesh than the standard KinFu mesh.

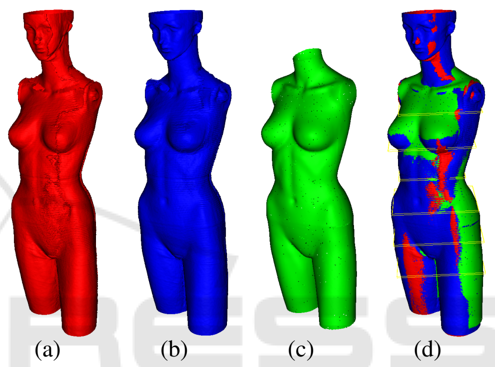

Figure 6: Reconstructed meshes comparison: (a) standard KinFu, (b) optimized KinFu, (c) ground truth meshes, (d) registered meshes and positions of some slices taken to show scaling effect.

In the second experiment, optimized KinFu is compared to standard KinFu for objects with high geometric shapes. In this experiment we used a styropor box with high geometric details as shown in Figure 8. While rotating the box in front of the camera using a turntable the depth frames are stored and then used to reconstruct a 3D model of the box using standard and optimized KinFu. As shown in Figure 8, the quality of the optimized KinFu mesh outperforms the quality of KinFu mesh. By comparing the second and the third row in Figure 8, it is clear that many fine details have been preserved in our optimized mesh, while they are blurred in the other mesh.

5 CONCLUSIONS

In this paper, we have presented a method to optimize KinectFusion method for 3D body scanning, where camera pose is described as a rotation about fixed axis passing through a fixed point. The camera motion tracking was split into two stages, the first one is

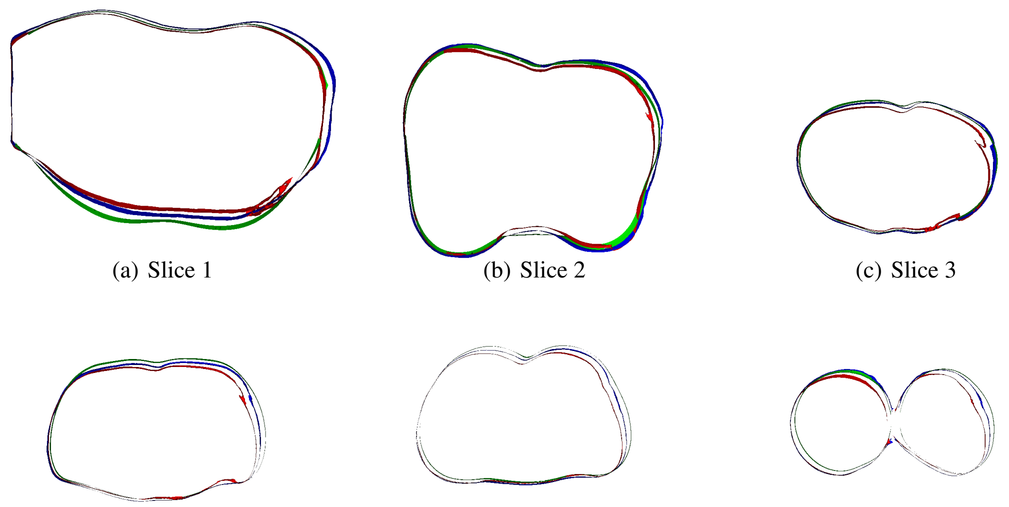

(a) Slice 1 (b) Slice 2 (c) Slice 3

(d) Slice 4 (e) Slice 5 (f) Slice 6

Figure 7: 2D views of slices from Fig 6(d): green shows ground truth, red shows standard KinFu, and blue shows optimized KinFu.

offline determining of rotation axis and center while reducing errors by noise averaging technique. The second one performs camera motion tracking limited to estimate only a rotation angle instead of estimating a complete 6 DoF transformation. Noise averaging in the first stage, and correspondence outliers removing through motion tracking limitation to on-dimensional in the second stage enhanced the quality of generated 3D model significantly as shown in the experimental results.

ACKNOWLEDGEMENTS

This work was supported by the German Federal Ministry of Education and Research (BMBF) under grant No. 03FH053PX5.

REFERENCES

Afzal, H., Ismaeil, K., Aouada, D., Destelle, F., Mirbach, B., and Ottersten, B. (2014). Kinect Deform: Enhanced 3D reconstruction of non-rigidly deforming objects. In *3DV (Workshops)*, pages 7–13. IEEE.

Arya, S., Mount, D. M., Netanyahu, N. S., Silverman, R., and Wu, A. Y. (1995). Registering multiview range data to create 3D computer objects. *IEEE Transactions on Pattern Analysis and Machine Intelligence (PAMI)*, 17(8):820–824.

Changchang, W. (2013). Towards linear-time incremental structure from motion. In *3DTV-Conference, 2013 International Conference on*, pages 127–134. IEEE.

Davison, A., Reid, I. D., Molton, N., and Stasse, O. (2007). MonoSLAM: Real-Time Single Camera SLAM. *IEEE Trans. Pattern Anal. Mach. Intell.*, 29(6):1052–1067.

Engel, J., Stückler, J., and Cremers, D. (2015). Large-scale direct SLAM with stereo cameras. In *In Proceedings of the IEEE International Conference on Intelligent Robots and Systems (IROS)*.

Fioraio, N. and Stefano, D. L. (2014). SlamDunk: affordable real-time RGB-D SLAM. In *Workshop at the European Conference on Computer Vision*, pages 401–414. Springer.

Furukawa, Y. and Ponce, J. (2007). Accurate, dense, and robust multi-view stereopsis. In *CVPR*. IEEE Computer Society.

Girardeau-Montaut, D. (2014). Cloudcompare.

Harris, M., Sengupta, S., and Owens, J. (2007). Parallel prefix sum (scan) with CUDA. In Nguyen and Hubert, editors, *GPU Gems 3*, chapter 39, pages 851–876. Addison Wesley.

Hernández, C., Vogiatzis, G., and Cipolla, R. (2007). Probabilistic visibility for multi-view stereo. In *CVPR*. IEEE Computer Society.

Izadi, S., Kim, D., Hilliges, O., Molyneaux, D., Newcombe, R., Kohli, P., Shotton, J., Hodges, S., Freeman, D., Davison, A., and Fitzgibbon, A. (2011). Kinectfusion: real-time 3D reconstruction and interaction using a moving depth camera. In *In Proc. UIST*, pages 559–568.

Jia, S., Li, B., Zhang, G., and Li, X. (2016). Improved kinectfusion based on graph-based optimization and large loop model. In *IEEE International Conference on Information and Automation (ICIA))*.

Kainz, B., Hauswiesner, S., Reitmayr, G., Steinberger, M., Grasset, R., Gruber, L., Veas, E. E., Kalkofen, D., Seichter, H., and Schmalstieg, D. (2012). OmniKi-

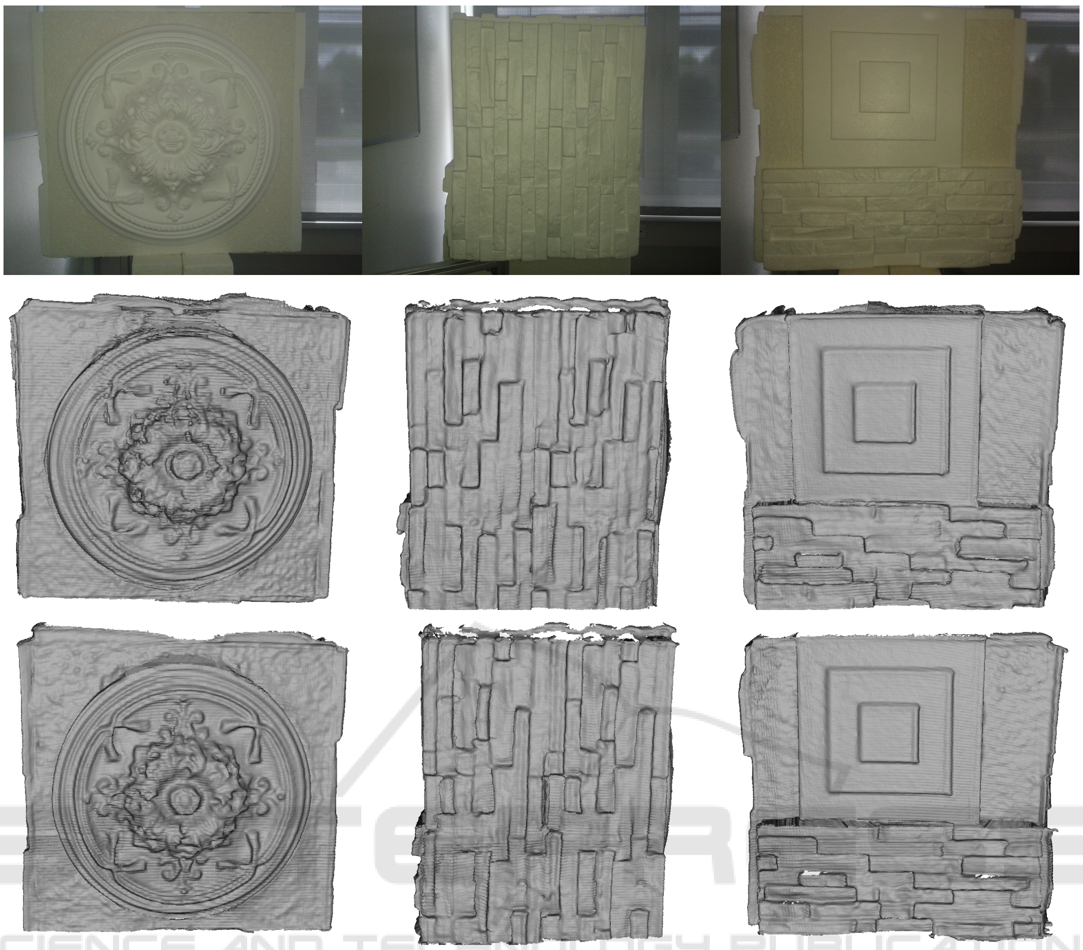
Figure 8: Comparison between standard and optimized KinFu for objects with high geometric features. First row: RGB images of 3 different sides of a box. Second row: box mesh reconstructed by KinFu. Third row: the same mesh reconstructed by optimized KinFu.

nect: real-time dense volumetric data acquisition and applications. In *VRST*, pages 25–32. ACM.

Kerl, C., Sturm, J., and Cremers, D. (2013). Dense visual SLAM for RGB-D cameras. In *Proc. of the Int. Conf. on Intelligent Robot Systems (IROS)*.

Moulon, P., Monasse, P., and Marlet, R. (2013). Global fusion of relative motions for robust, accurate and scalable structure from motion. In *Proc. ICCV*. IEEE.

Negre, P. L., Bonin-Font, F., and Oliver, G. (2016). Cluster-based loop closing detection for underwater SLAM in feature-poor regions. In *2016 IEEE International Conference on Robotics and Automation (ICRA)*, pages 2589–2595.

Newcombe, R., Izadi, S., Hilliges, O., Molyneaux, D., Kim, D., Davison, A., Kohli, P., Shotton, J., Hodges, S., and Fitzgibbon, A. (2011). Kinectfusion: Real-time dense surface mapping and tracking. In *Proc. IEEE Int. Symp. Mixed and Augm. Reality*. IEEE.

Ni, K., Steedly, D., and Dellaert, F. (2007). Out-of-core bundle adjustment for large-scale 3D reconstruction. In *International Conference on Computer Vision (ICCV)*.

Pagliari, D., Menna, F., Roncella, R., Remondino, F., and Pinto, L. (2014). Kinect fusion improvement using depth camera calibration. In *the Technical Commission V Symposium Remote Sensing Spatial and Information Science*, pages 23–25.

Schoeps, T., Engel, J., and Cremers, D. (2014). Semi-dense visual odometry for AR on a smartphone. In *ismar*.

Whelan, T., Kaess, M., Fallon, M., Johannsson, H., Leonard, J., and McDonald, J. (2012). Kintinuous: Spatially extended kinectfusion. In *RSS Workshop on RGB-D: Advanced Reasoning with Depth Cameras*, Sydney, Australia.

Wiedemeyer, T. (2014–2015). Iai kinect2. Accessed June 12, 2015.

Yang, C. and Gerard, M. (1992). Object modelling by registration of multiple range images. *Image Vision Comput.*, 10(3):145–155.

Yu, W. and Zhang, H. (2016). 3D Reconstruction of Indoor Scenes Based on Feature and Graph Optimization. In *International Conference on Virtual Reality and Visualization (ICVRV)*. IEEE.